American Mineralogist, Volume 74, pages 1070–1083, 1989

Transmission electron microscopy of interfaces and defects in intergrown pyroxenes

KENNETH J. T. LIVI, DAVID R. VEBLEN
Department of Earth and Planetary Sciences, The Johns Hopkins University, Baltimore, Maryland 21218, U.S.A.

ABSTRACT

High-resolution and conventional transmission electron microscopy has been used to study exsolved augites from the Laramie Anorthosite Complex, and the HRTEM images have been interpreted through extensive computer-generated image simulations. The results illustrate the complexity of interface structures and morphologies in exsolved pyroxenes and confirm that defects such as dislocations and stacking faults play an important role in pyroxene exsolution processes.

Pigeonite in the Laramie augite occurs as both "100" and "001" lamellae, and the degree of coherency of the interfaces is inversely related to the lamellar size. Both sets of lamellae grew by the propagation of growth ledges, and HRTEM images of the dislocations on "100" growth ledges are consistent with unit Burgers vectors of [001]. The interfaces of "001" pigeonite lamellae have a stepped morphology where they intersect (100) stacking faults in the pigeonite; the faults have the stacking sequence $+--+$ and therefore can be described as single blocks of orthopyroxene structure. The $^{1}/_{2}$[001] partial dislocations at the terminations of the stacking faults are dissociated into two equal partials approximately 5 nm apart, and the stacking sequence of the faults between the two partials is $+-+$. Where "100" and "001" pigeonite lamellae approach each other, the "100" lamellae typically have bulges on both sides, and the "001" lamellae are hooked, probably at least partially because of interaction between the strain fields of the growing lamellae. In an additional unrelated observation, narrow orthopyroxene lamellae grew from their tips as entire lamellae, rather than by a ledge mechanism. Each growing orthopyroxene unit cell is led by two partial dislocations, the strain fields of which cancel each other.

Most of the stacking faults observed in orthopyroxene involved skew reversal of an even number of (100) octahedral layers, and most of the faults observed in pigeonite also consisted of even numbers of octahedral layers and were separated by slabs of ordinary pigeonite containing an even number of octahedral layers. However, a number of odd-layered faults also were observed in both orthopyroxene and pigeonite, indicating that a full description of the stacking phenomena in real pyroxenes requires the use of 0.45-nm (100) slabs of structure, rather than the 0.9-nm layers used by some authors. HRTEM images indicate that the stacking faults in pigeonite nucleate symmetrically about the B chains of the pigeonite structure. The structures and distribution of the stacking faults show that their positions are structurally controlled and confirm that they formed below the $C2/c \rightarrow P2_1/c$ transition temperature.

INTRODUCTION

It has been long recognized that rock-forming pyroxenes commonly exhibit a wide variety of intergrowth structures that result from exsolution (also called precipitation) (Poldervaart and Hess, 1951; see also review by Buseck et al., 1980). Although these intergrowths in orthopyroxene, augite, and pigeonite were initially reported to form in rational orientations parallel to (001) and (100), it is now recognized that these intergrowth orientations are variable, that they depend on the detailed crystal structures and unit-cell parameters at conditions of nucleation and during growth, and that exsolution microstructures observable with the petrographic microscope can be quite complex (e.g., Robinson et al., 1977; Robinson, 1980). Furthermore, transmission electron microscopy (TEM) studies have demonstrated that features below the resolution of the light microscope, such as growth ledges, stacking faults, and interface dislocations, can play an important role in the development and thermal equilibration of pyroxene intergrowths during cooling or annealing (Champness and Lorimer, 1976; Nord et al., 1976; Iijima and Buseck, 1975; Kohlstedt and Vander Sande, 1976; Champness and Copley, 1976; Robinson et al., 1977; Buseck et al., 1980; Kitamura et al., 1981a; Nord, 1980, 1982; Nobugai and Morimoto, 1979; Rietmeijer and Champness, 1982; Crawford et al., 1983; Mori and Takeda, 1988). These features are in general a

0003–004X/89/0910–1070$02.00

response to the strain involved in the fitting together of the host and precipitate structures.

Most of the TEM studies of pyroxene exsolution phenomena have been performed using conventional bright- and dark-field imaging techniques or one-dimensional lattice imaging of fringes parallel to (100). In the present paper, we present results of [010] two-dimensional high-resolution TEM (HRTEM) experiments on exsolved augites from the Laramie Anorthosite Complex (Livi, 1987). In order to interpret such images reliably, we have performed extensive computer simulations of the HRTEM images under a wide variety of imaging conditions. The experimental images reveal previously unresolved details of quadrilateral-pyroxene interface structures and allow interpretation of exsolution mechanisms for the Laramie pyroxenes. In addition, we present conventional TEM observations on unusual lamellar morphologies that result from interactions among crystallographically different sets of exsolution lamellae.

Sample description and experimental methods

Exsolved augites in sample LAC-6A from the fine-grained ferromonzonite border facies of the Laramie Anorthosite Complex have been described by Livi (1987), Fuhrman et al. (1988), and Frost and Lindsley (1981). The Fe-rich augite crystals are anhedral to subhedral, range up to 3 mm in diameter, and exhibit a variety of exsolution textures. Livi (1987) described in detail the chemistry and texture of subsolidus structures pertinent to the investigation of the augite cooling history, identifying most of the exsolved lamellae as very low Ca pigeonites and noting the presence of small numbers of orthopyroxene lamellae. Although the lamellae exhibit a wide range of sizes and orientations, their compositions indicate that all lamellae have re-equilibrated at 600 to 650 °C.

The present paper describes further observations on the microstructures present in LAC-6A augites. Thin specimens were prepared using standard Ar-ion milling techniques and were lightly coated with C. Low-resolution TEM was performed with a JEOL 200CX electron microscope at the State University of New York at Stony Brook using procedures reported by Livi (1987). HRTEM was performed with a Philips 420ST microscope at The Johns Hopkins University. Optical conditions for the Philips microscope are described by Livi and Veblen (1987). Proper specimen orientations for HRTEM imaging were obtained with a 3-mm Philips double-tilt specimen holder, and images presented here were recorded at magnification settings of between 730 000× and 1 230 000×.

Two-dimensional imaging of pyroxenes parallel to their *b* axes requires resolution of the (002) fringes, which have spacings of approximately 0.25 nm. Since this spacing is beyond the Scherzer limit of our microscope (0.30 nm), intuitive interpretation of the HRTEM images is not possible, necessitating the use of computer-simulation methods to interpret the imaging results. Simulated high-resolution images of *b*-axis micrographs were calculated using the 80F version of the SHRLI programs (Self and O'Keefe, 1988; O'Keefe et al., 1978). The halftone output routines were modified for use with a dot-matrix graphics line printer. The calculation of electron-diffraction amplitudes and phases was fully dynamical, using the multislice formulation of Cowley and Moodie (1957).

The input structures for the image simulations were those refined by Cameron et al. (1973) for augite, by Smyth (1973) for orthopyroxene, by Morimoto and Koto (1969) for another orthopyroxene and a model in which clinohypersthene was twinned into the ortho structure, and by Smyth (1974) for clinohypersthene. Cation occupancies were altered for consistency with the pyroxene compositions observed in LAC-6A (Livi, 1987). There were no appreciable differences in calculated images for the two refinements of orthopyroxene, nor were there between the calculated images for the orthopyroxenes and the model twinned clinohypersthene. The orthopyroxene calculations shown here are for the Smyth (1973) structure. It was found that varying the model slice thicknesses did not result in noticeable differences in the simulated images; as a result, a slice thickness equal to the length of the *b* axis was utilized for most calculations. The simulations were required to match the experimental images of two different structures observed at interfaces under identical conditions of defocus, crystal thickness, and orientation. It was found that the imaging conditions are highly constrained by this requirement of matching the experimental and computer-simulated images of two structures.

Image simulations

Figure 1 presents selected simulation results for augite, pigeonite, and orthopyroxene images viewed down the *b* crystallographic axis at various focus settings and at crystal thicknesses of 4.5 and 9.0 nm. It was necessary to calculate images at defocus intervals of approximately 5 nm, since the image character can change significantly with small changes in focus. However, owing to space limitations, Figure 1 presents only selected simulations that generally illustrate the manner in which pyroxene images change with focus and thickness for a microscope with the optical characteristics of the Philips 420ST (i.e., point-to-point resolution of approximately 0.3 nm).

Contrast details of simulated images

The correspondence of simulated-image characteristics to the pyroxene structures can be summarized as follows. With crystals 4.5-nm thick, focus settings between +20 and 0 nm produce white spots that lie close to the planes of the octahedral sheets, either over or between the octahedral cation positions (see +20-nm images). At focuses from approximately −20 to −65 nm, lines of white spots lie over the tetrahedral chains. At −65 nm, the more prominent lines of dots correspond to the positions of the A chains for both the pigeonite and the orthopyroxene structures. The B-chain spots for pigeonite and orthopyroxene and the spots for augite are all tilted, and

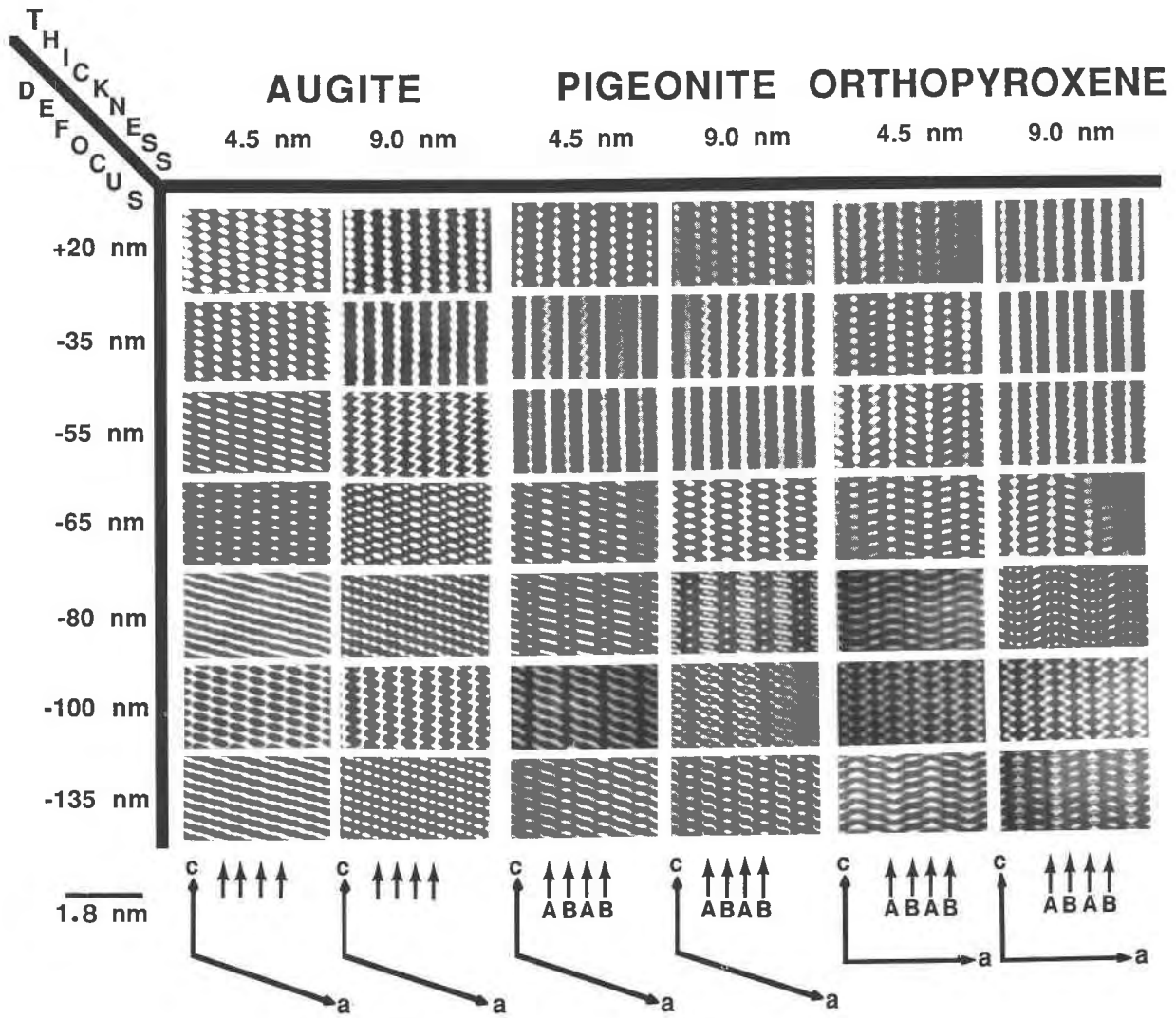

Fig. 1. Representative computer-simulated *b*-axis HRTEM images for augite, pigeonite, and orthopyroxene at crystal thicknesses of 4.5 and 9 nm and at various focus settings. The vertical arrows denote positions of the tetrahedral chains. A and B refer to the chain type. A 1.8-nm scale bar is in the lower left corner of the diagram.

the tilt direction of the spots indicates the skew of the adjacent octahedral strips (see Thompson, 1981, p. 146, for a definition of the + and − stacking vectors that denote the direction of octahedral skew). It is thus possible, at least in principle, to determine the exact stacking sequence of a pyroxene from images taken under focus values near −65 nm. At defocus values of approximately −90 to −130 nm, the brightest spots in the image again lie in or near the planes of the octahedral sheets, either over or between the octahedral cations. At greater defocus values, the bright spots switch back to the tetrahedral chains.

The orthopyroxene simulations in Figure 1 show even intensity of alternate (100) rows of spots (i.e., an apparent 0.9-nm periodicity parallel to the *a* axis in the *intensities* of the rows of spots). However, experimental high-resolution images commonly exhibit an asymmetry in the sizes and intensities of the spots corresponding to alternate (100) layers of A chains, even though these layers are symmetrically identical. Our diffraction calculations show that in the case of an orthopyroxene crystal perfectly oriented down the *b* axis and a parallel (i.e., not convergent) incident beam, dynamical scattering (multiple diffraction) into the 100 beam is negligible. Thus, under such ideal illumination conditions, those diffracted beams that are kinematically forbidden by the orthopyroxene *a*–glide plane (e.g., the 100 beam) would have very low intensities. Since it is primarily these odd-order *h*00 diffractions that contribute to the image information with 1.8-nm periodicity, the resulting images exhibit only a symmetric 0.9-nm periodicity in spot intensities.

In order to determine the cause for the differences be-

tween calculated and experimental orthopyroxene images, we performed a series of simulations in which a parallel electron beam was tilted slightly with respect to the orthopyroxene *b* axis. The calculations at −65-nm defocus and 4.5-nm crystal thickness (Fig. 2a) demonstrate that in extremely thin crystals, the rows of dots corresponding to alternating (100) layers of A chains become unequal in intensity. Alternate layers of B chains likewise become asymmetrical, though not so noticeably. However, the changes in spot size and intensity for thin crystals are minor compared to those for thicker crystals (Fig. 2b). This is because dynamical diffraction becomes more important with increasing crystal thickness. Inspection of the dynamical intensities indicates that the odd-order *h*00 intensities become appreciable for crystals 9-nm thick, and this is reflected in the pronounced asymmetry in spot intensities seen in some of the images of Figure 2b. Yet, when the images calculated for the central beam tilted in the direction of the 004 and 00$\bar{4}$ beams (approximately 4 milliradians or 1.4° off-axis) are compared, the positions of the large and small spots are reversed. An image formed from a convergent beam (a cone of illumination containing a symmetrical range of angles of incident electrons) and a perfectly oriented crystal should thus be a summation of images of opposite intensity and therefore should have spots of even sizes and intensities lying over all layers of A chains. We must conclude, therefore, that the asymmetry in many of our orthopyroxene images is due to small crystal misorientations or slight misalignments in the illumination system. Such images can still be interpreted with the aid of computer-generated image simulations.

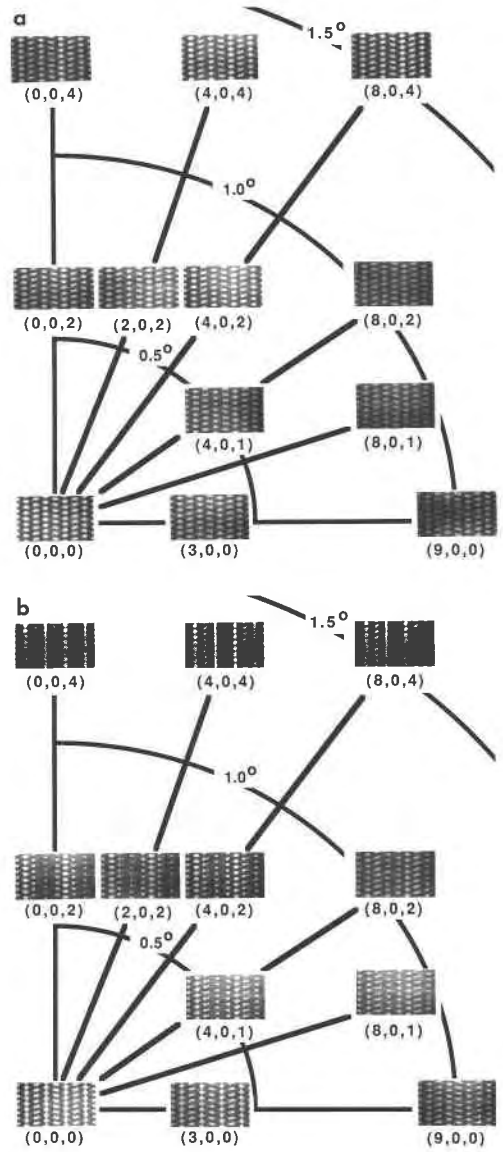

Fig. 2. **(a)** Simulated tilt matrix showing the effects of slight crystal misorientations on HRTEM images from a 4.5-nm-thick orthopyroxene crystal at a focus setting of −65 nm. Numbers in parentheses indicate the indices of the diffracted beam that was parallel to the *b* axis for each simulation. **(b)** Simulated HRTEM tilt matrix as in part a, but for a 9-nm-thick crystal.

Matches of simulated and experimental images

Calculated images of augite, pigeonite, and orthopyroxene are compared with experimental images in Figures 3a, 3b, and 3c. Since defocus values of −55 to −80 nm create images with high contrast and are near the optimum (Scherzer) defocus value for the microscope, most high-resolution images were recorded at these conditions. The excellent matches for augite and pigeonite were obtained at −63-nm defocus and 4.5-nm thickness. The experimental image of orthopyroxene in Figure 3a shows the asymmetrical spots mentioned above. An image calculated with the central electron beam parallel to the orthopyroxene 802 beam direction, −65-nm defocus, and 9.0-nm thickness matches relatively well with the illustrated experimental image.

The important features to note in images obtained under these conditions are as follows: (1) the white dots lie over the silicate chains; (2) the sizes of the dots can be used to distinguish between the A and B chains in pigeonite and orthopyroxene; and (3) in slightly misoriented orthopyroxene, alternate A chains produce different contrast.

Pyroxene interfaces

As noted above, the Fe-rich augite LAC-6A contains abundant exsolution lamellae of pigeonite and relatively few orthopyroxene lamellae. At the level of resolution of the petrographic microscope, orthopyroxene lamellae are not observed, but TEM observations indicate that narrow lamellae are present and are rigorously parallel to (100) of the host augite. With the petrographic microscope, it is observed that pigeonite lamellae lie in orientations that deviate slightly from (100) and (001), as described by Livi (1987); these are referred to as "100" and "001" lamellae. Such deviations of lamellar orientations from (100) and (001) are typical of exsolved augites (Robinson, 1980).

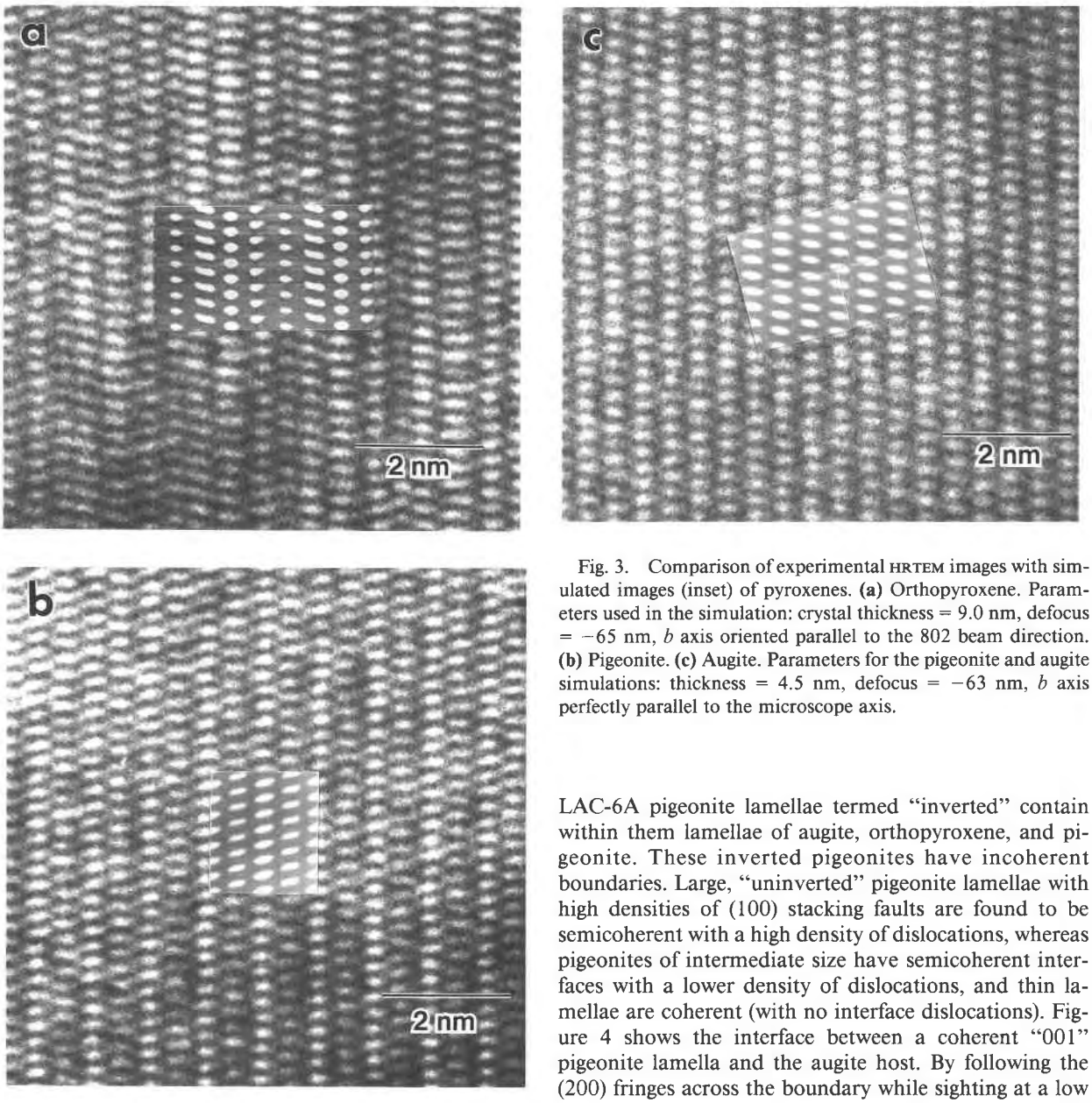

Fig. 3. Comparison of experimental HRTEM images with simulated images (inset) of pyroxenes. **(a)** Orthopyroxene. Parameters used in the simulation: crystal thickness = 9.0 nm, defocus = −65 nm, *b* axis oriented parallel to the 802 beam direction. **(b)** Pigeonite. **(c)** Augite. Parameters for the pigeonite and augite simulations: thickness = 4.5 nm, defocus = −63 nm, *b* axis perfectly parallel to the microscope axis.

Augite-pigeonite interfaces

Pigeonite lamellae in LAC-6A augites are typical of exsolved pigeonites found in other studies in that they have growth ledges, stacking faults, and dislocations at their boundaries (Copley et al., 1974; Champness and Copley, 1976; Nord et al., 1976; Robinson et al., 1977; Rietmeijer and Champness, 1982). These features will be addressed in light of two-dimensional pyroxene lattice imaging. More unusual features such as bulging and hooking of lamellae will be discussed in a later section.

The pigeonite lamellae in LAC-6A augites exhibit a range of interface coherency with the host augite. A few LAC-6A pigeonite lamellae termed "inverted" contain within them lamellae of augite, orthopyroxene, and pigeonite. These inverted pigeonites have incoherent boundaries. Large, "uninverted" pigeonite lamellae with high densities of (100) stacking faults are found to be semicoherent with a high density of dislocations, whereas pigeonites of intermediate size have semicoherent interfaces with a lower density of dislocations, and thin lamellae are coherent (with no interface dislocations). Figure 4 shows the interface between a coherent "001" pigeonite lamella and the augite host. By following the (200) fringes across the boundary while sighting at a low angle, it can be seen that the two (100) planes are at a small angle to each other, while the (002) fringes in pigeonite and augite are parallel. These relations show that thin "001" pigeonites have their *a* axes parallel to those of the augite host, but the *c* axes are tilted. Similar images of thin "100" pigeonite lamellae show that the (200) fringes of host and lamellae are parallel, indicating that the *c* axes are parallel, but the *a* axes are not parallel. These orientation relationships between the two lattices are consistent with those observed previously with other methods (Buseck et al., 1980; Robinson, 1980).

Figure 4 also shows that the augite (200) fringes bend in a subtle "s" fashion over the space of several unit cells before reaching the augite/pigeonite boundary distinguished by the meeting of the two pyroxenes' distinctive

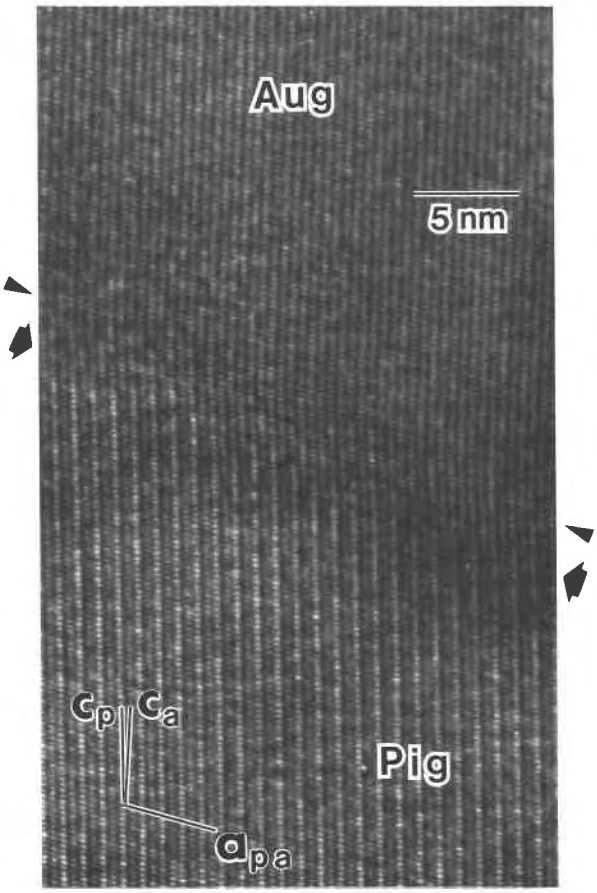

Fig. 4. A *b*-axis HRTEM image showing relative axial orientation and bending of fringes at the coherent interface of a "001" pigeonite-augite exsolution lamella. The lower set of arrows indicates the trace of the boundary, and the upper set indicates where most of the bending of fringes takes place.

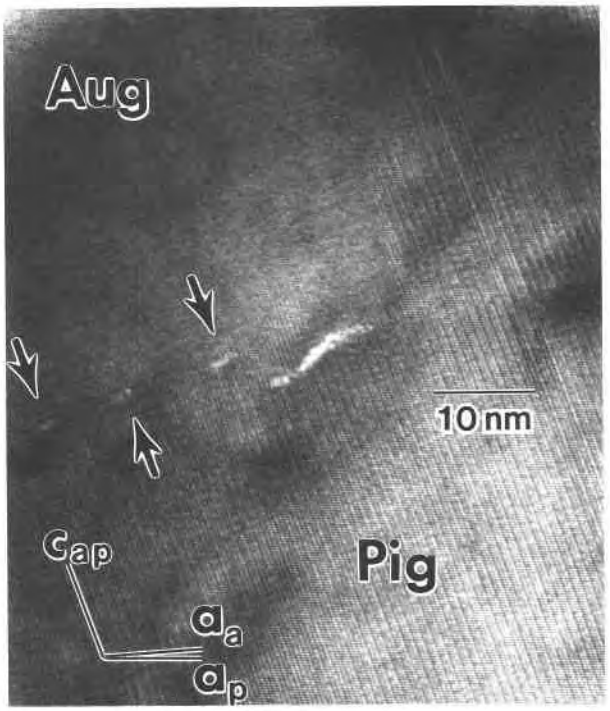

Fig. 5. A *b*-axis HRTEM image of dislocations with projected Burgers vector 1[001] (arrowed) on a very large growth ledge of a "100" pigeonite lamella. The "100" lamella contains a pair of (100) stacking faults. The large defect in the center that is not arrowed is a combination of more than one dislocation and has a resultant Burgers vector of [201].

image contrast. The major portion of the bending occurs approximately six augite unit cells from the boundary. This suggests that the strain of fitting the two structures together is distributed over a distance of a few nanometers from the actual boundary. This bending contrasts with the assumption of the exact-phase-boundary theory for pyroxenes, in which two rigid lattices are matched by varying orientations of the interfaces and the lattices (e.g., Robinson et al., 1977). However, as shown by Livi (1987), the exact-phase-boundary hypothesis does explain the trends among size, orientation, and history of pigeonite lamellae in LAC-6A augites. The exact-phase-boundary theory therefore may not be seriously affected by lattices that are not completely rigid and interface regions that are several nanometers in width, rather than being a discrete interface plane. It obviously is not known whether or not the boundary also involves a gradation or an abrupt change in chemistry.

Previous studies of augite-pigeonite grain boundaries have demonstrated that "100" pigeonite lamellae in augite hosts thicken by means of growth ledges (Champness and Lorimer, 1973; Copley et al., 1974; Kitamura et al., 1981a). However, the dislocations found at the tips of ledges have not been fully characterized previously. Figure 5 shows a two-dimensional lattice image of an unusually wide growth ledge on a "100" pigeonite lamella in the LAC-6A augite. Enlargements of such images allow the construction of Burgers circuits around these defects. The projected Burgers vector thus determined to be associated with "100" growth ledges is 1[001]. Nord et al. (1976) have shown that unit dislocations with this Burgers vector provide good nucleation sites for "100" pigeonite lamellae. Nucleation of secondary pigeonite lamellae on these ledges at lower temperatures may thus account for the branching "100" lamellae observed in this augite (see Fig. 4 of Livi, 1987).

Stacking faults and associated dislocations in "001" pigeonite

Stacking faults rigorously parallel to (100) are found commonly in pigeonite lamellae. Many studies have investigated the nature of similar stacking faults in a variety of pyroxenes and have suggested that they can be described as unit-cell scale twins with displacement vectors $^{1}/_{12}$[001] (Champness and Copley, 1976; Coe and Kirby, 1975; Iijima and Buseck, 1975; McLaren and Etheridge, 1976). Robinson et al. (1977) observed stacking faults in

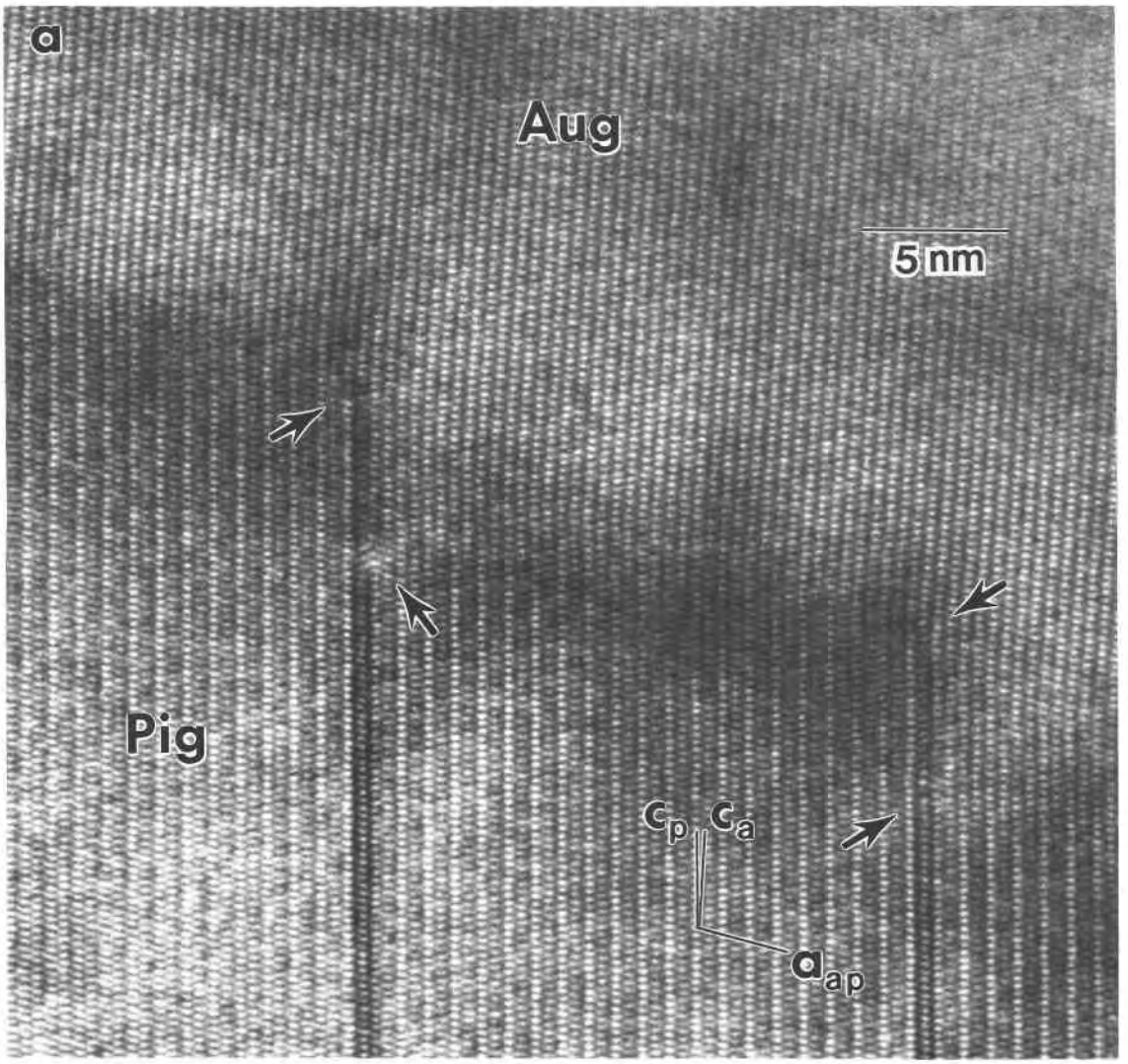

Fig. 6. **(a)** HRTEM image of stacking faults in pigeonite terminating at a "001" pigeonite-augite boundary. The arrows point to the dissociated partial dislocations at the tips of the stacking faults. Steps in the interface associated with the stacking faults are evident, and the rotation of *c* axes across the interface can be seen clearly by viewing at a low angle parallel to *c*.

"001" pigeonite lamellae that terminate at the interface with augite, similar to the faults observed in the present study. They argued persuasively that the stacking faults form during cooling, in order to minimize the strain energy in response to the changing pigeonite and augite unit-cell parameters.

We have obtained HRTEM images from LAC-6A, as given in Figure 6a, that show in detail the stacking faults, the dislocations at their terminations, the distribution of augite and pigeonite in the neighborhood of the terminations, as well as the lattice rotation previously discussed. Burgers circuits constructed around stacking-fault terminations on the HRTEM images confirm a projected Burgers vector of approximately $^{1}/_{12}[001]$. However, the images also show that the partial dislocations pinned at the boundaries of the lamellae are dissociated into two equal partial dislocations with Burgers vectors of $^{5}/_{12}[001]$. A schematic diagram illustrating such a Burgers circuit and the two partials is given in Figure 6b. The partial dislocations are generally separated by about 5 nm; the dissocation into partial dislocations probably has not been observed previously because the resolution of conventional bright- and dark-field TEM experiments is typically on the order of 5 nm. The dissociation of the interface dislocations suggests that the formation of a stacking fault may take place in two steps; the passage of each partial dislocation through the structure produces a relative shift between two adjacent (100) sheets of oxygen atoms of $^{5}/_{12}[001]$. The images also show that between the partial dislocations, the stacking faults separate augite on one side from pigeonite on the other, producing steps in the pigeonite-augite interface.

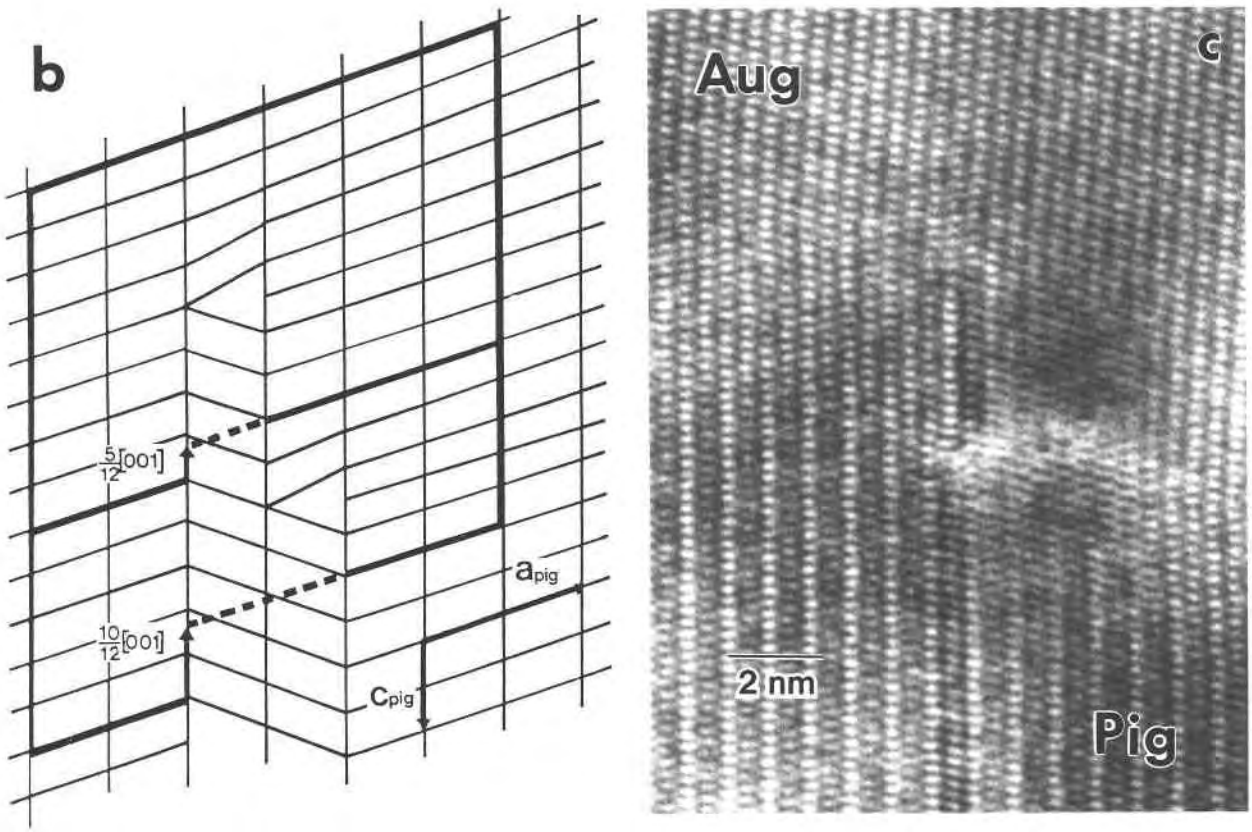

Fig. 6—*Continued.* **(b)** Schematic diagram showing Burgers circuits around the termination of a stacking fault in pigeonite, illustrating the splitting of the fault into two equal partial dislocations. The portion of the fault between the partials is a single-layered fault with structure $+-+$, whereas the stacking fault at the bottom of the figure has the more normal structure $+--+$. **(c)** HRTEM image of the termination of a stacking fault in which the region between the two dissociated partial dislocations involves an antiphase boundary.

The stacking sequence of an unfaulted clinopyroxene crystal can be represented as (+), indicating that all octahedra have the same skew; the sequence of stacking vectors is placed in parentheses to indicate that it repeats periodically (see Thompson, 1981, p. 146, and Veblen, 1981, p. 194, for definitions and usage of + and − polytype nomenclature). The normal stacking fault structure that we observe in these pigeonites can be represented as $+--+$, indicating that the fault involves reversal of the skew for two adjacent octahedral sheets (this sequence is not placed in parentheses, indicating that it is a fault structure and does not repeat periodically). We refer to this type of stacking fault as a two-layer fault, or an even-layered fault, because it contains an even number of octahedral layers. This type of stacking fault also could be described as a single unit cell of orthopyroxene structure, since the normal orthopyroxene stacking can be represented as a periodic repetition of the sequence $(+--+)$. Between the two partial dislocations, however, the stacking fault has the structure $+-+$, which could be described as a single unit cell of protopyroxene structure, since the proto stacking sequence is $(+-)$. Because this latter type of stacking fault involves skew reversal of only a single octahedral layer, we refer to it as a one-layer fault, which is one type of odd-layered fault. In a later section, we discuss the frequency of occurrence of even- and odd-layered faults in rock-forming pyroxenes.

Figure 6c shows an additional complication observed at one stacking fault termination at a "001" pigeonite-augite interface. Not only does the stacking fault dissociate into two partials, but the type of tetrahedral chain (A or B) appears to change between the two dislocations, producing a short antiphase boundary in the pigeonite along the one-layer section of stacking fault. It is not known how common this structure is, since the number of terminating stacking faults found in areas thin enough for HRTEM imaging was small.

Dissociated partial dislocations are common in metals, and their presence in these pyroxenes is not surprising, since the clinopyroxene structure permits splitting of the whole dislocation. For a given Burgers vector direction, the energy of a dislocation is approximately proportional to the square of the Burgers vector magnitude $|\mathbf{b}|^2$ (e.g., Hull, 1965, p. 78). Therefore, the total dislocation energy may be reduced by approximately one-half if the dislocation can be dissociated into two parts. Since both Bur-

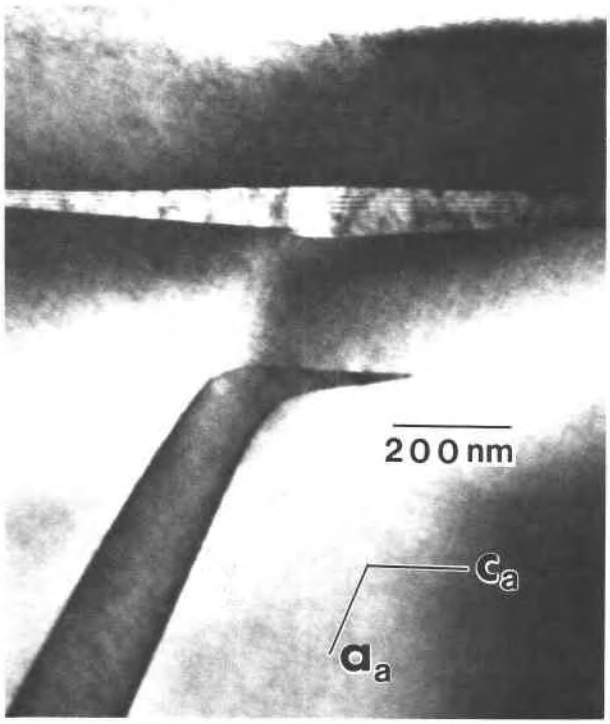

Fig. 7. TEM image of hooked "001" and bulging "100" pigeonite lamellae in augite. By viewing at a low angle parallel to the "100" lamella, it can be seen that bulging occurs on both sides. Fine lines in this lamella are stacking faults.

gers vectors have the same sign, the partial dislocations should repel each other. The distance between the partials is a balance between the repulsive forces that arise from elastic interaction and the attractive force represented by the energy of the $+-+$ stacking fault between the partials. The distances observed between the paired partials were relatively constant at 10 to 11.5 $\times$ c, or 5.2 to 6.0 nm, suggesting that the dissociated configuration adopted by these interface dislocations represents an energy minimum. HRTEM or weak-beam TEM observations of dislocations at augite-pigeonite interfaces in other occurrences, such as those shown in Figure 12 of Robinson et al. (1977), would clarify whether or not such a dissociated dislocation structure is the usual one for "001" pigeonite lamellae with (100) stacking faults. Likewise, further work using HRTEM or weak-beam techniques will be necessary to determine if the dislocations associated with stacking faults involved in structural phase transformations in low-Ca clinopyroxenes and orthopyroxenes (e.g., Müller, 1974; Coe and Kirby, 1975; Buseck and Iijima, 1975; McLaren and Etheridge, 1976) are dissociated.

Morphology of pigeonite lamellae

Several studies have indicated that pigeonite exsolution lamellae in Fe-rich augites can have complex morphologies not observed in more Mg-rich pyroxenes. These unusual lamellae either terminate with an obtuse-angled hook or have peculiar bulges that are spatially related to neighboring lamellae (Kitamura et al., 1981b; Rietmeijer and Champness, 1982; Livi and Veblen, 1984). Figure 7 shows a typical pair of lamellae that exhibit these features. In LAC-6A augite, hooking occurs exclusively in "001" pigeonite lamellae that are near "100" pigeonite lamellae. Bulging is only present in "100" pigeonite lamellae in the vicinity of hooking lamellae. This bulging occurs on both sides of the "100" lamellae, even when there is a hooked "001" on only one side. It is observed that "100" lamellae impinging on "001" lamellae do not result in bulging of the "001" lamellae.

Suitable explanations for this texture should satisfactorily take into account all of these features. The investigators mentioned above all suggest that changes in unit-cell parameters contribute to changes in preferred growth orientations (either "100" or "001"). Rietmeijer and Champness (1982) also speculated that solute-depleted zones at the borders of "100" lamellae interfere with the growth of approaching "001" lamellae. The hooks are then added at a lower temperature when the growth direction switches from "001" to "100." This hypothesis does not explain why hooking is always accompanied by bulging, which might not be expected to form in a solute-depleted zone.

Kitamura et al. (1981b) attributed lamellar hooking to a thermal interval (called the morphological change temperature, MCT) in which the direction of favored growth switches from "001" to "100." Lamellae growing in this temperature range will exhibit both "001" and "100" orientations. However, the MCT hypothesis does not account for the spatial relationship between hooked lamellae and "100" lamellae, nor does it explain why the "100" lamellae bulge in the presence of impinging "001" lamellae.

Although the models of Rietmeijer and Champness (1982) and Kitamura et al. (1981b) may explain hooking in some occurences, the spatial relationship between "001" hooking and "100" bulging suggests that these features result at least partially from the interacting strain fields of the two lamellae and from the resulting changes in energetically favored interface orientation. Similar strain field interactions arising between different twin orientations have been invoked to explain unusual, nonplanar lamellae in alkali feldspars (Salje et al., 1985). In the present case, a change in interface morphology could be due to local, strain-induced changes in the unit-cell parameters of the augite host that lies between the "100" and impinging "001" lamellae. If the strain field from a "001" lamella extends through the "100," then this could explain why bulging occurs on both sides of the lamellae. It is also possible that solute depletion contributes to hooking of "001" lamellae, as suggested by Rietmeijer and Champness (1982), whereas "100" bulging is the result of the strain field from the impinging "001."

As new growth proceeds, the hooked and bulged lamellae can join to form a hinge structure, as shown in Figure 8. All such hinge structures that we have observed

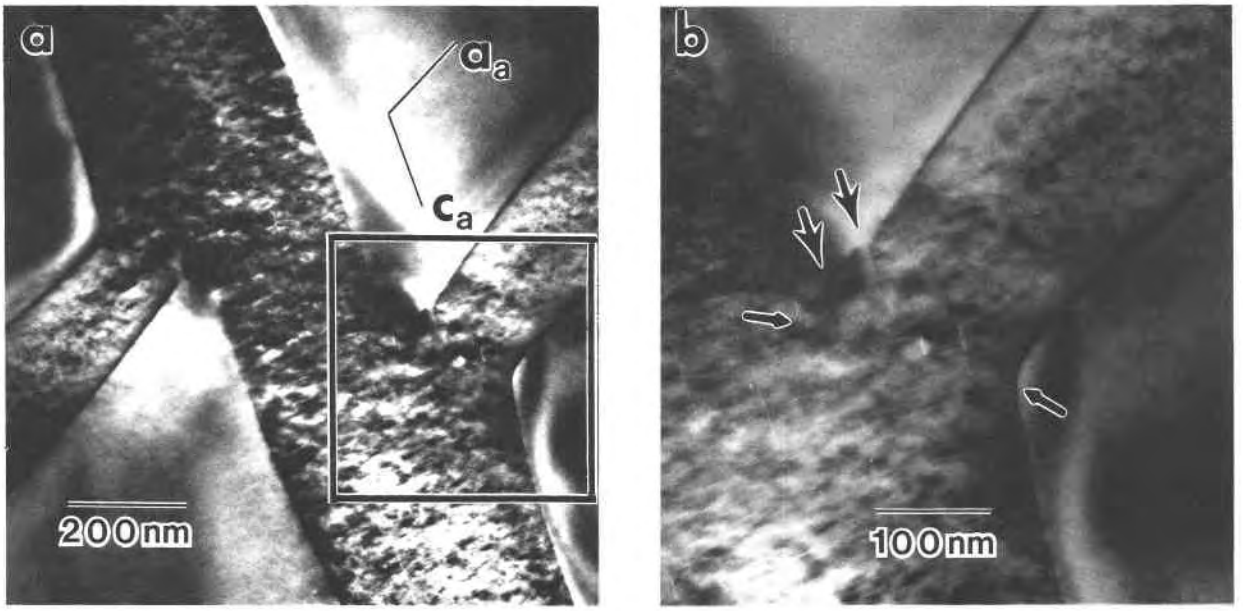

Fig. 8. **(a)** TEM image of intersecting "100" and "001" pigeonite lamellae. Boxed region is enlarged in part b. **(b)** Enlargement of the hinge region of one of the lamellar intersections shown in part a. The large arrows point to notches of augite included in the pigeonite hinge. The small arrows indicate a low-angle boundary between the "100" and "001" pigeonite lamellae; the boundary forms when the lamellae intersect, because "100" and "001" lamellae are oriented differently in the augite host.

in LAC-6A include a small sliver of host augite in the acute side of the hinge. The dislocations associated with these "notches" have Burgers vectors of 1[001], identical to those associated with growth ledges on "100" lamellae. These notches may represent Ca-rich pyroxene caught between impinging pigeonite lamellae.

Augite-orthopyroxene interfaces

Little orthopyroxene is present in LAC-6A, with the largest lamellae being only a few tens of nanometers wide. Figure 9a shows one lamella terminating in the augite host. A circuit constructed around the tip (shown schematically in Fig. 9b) indicates that the augite lattice is undisturbed, and there is no evidence of strain contrast in the augite. The growth of orthopyroxene from a monoclinic pyroxene host is thought to involve the propagation of $^{10}/_{12}$[001] partial dislocations (e.g., a Burgers vector of $^1/_6$[001] as suggested by Champness and Copley, 1976). Unfortunately, our HRTEM images do not shed any further light on the exact dislocation structure involved in this transformation. However, we can state that the interface at the lamellar tip is very tight, and the apparent absence of strain suggests that the strain fields of any dislocations involved in the growth of the orthopyroxene in LAC-6A may cancel each other, at least partially.

Previous studies of augite exsolution lamellae in orthopyroxene have suggested that the lamellae grow by a mechanism in which narrow ledges that are only one to four unit cells wide propagate along the lamellar interface (Champness and Lorimer, 1973; Vander Sande and Kohlstedt, 1974; Kohlstedt and Vander Sande, 1976). However, the termination of the entire orthopyroxene lamella in Figure 9a suggests that in this case of orthopyroxene exsolving from augite, the lamellae formed by collective growth of a larger number of orthopyroxene unit cells. Failure to observe ledges far from the tips of lamellae suggests that they did not coarsen following initial growth at the lamellar tip. However, such ledges could have been missed, given the low density of orthopyroxene lamellae in LAC-6A.

Structure and spacing of stacking faults in rock-forming pyroxenes

There have been numerous observations of (100) stacking faults in low-Ca clinopyroxenes and orthopyroxenes (for review, see Buseck et al., 1980). Such stacking faults commonly have been discussed in terms of the stacking of 0.9-nm structural slabs parallel to (100), for example, by Buseck and Iijima (1975). Such slabs, which are most conveniently defined as being bounded by planes within the layers of silicate chains of the pyribole structures, contain two layers of octahedral strips. As a result, we refer to stacking faults that can be fully described with such 0.9-nm slabs as even-layered faults. Two common examples of even-layered stacking faults in pyroxenes include (1) pairs of octahedral layers having reversed skew in clinopyroxenes, resulting in isolated blocks with $+--+$ structure, and (2) extra pairs of octahedral layers without skew reversal between the A chains of orthopyroxenes, resulting in blocks with $+----+$ structure. In addition, interpretation of the structure of pyroxenes

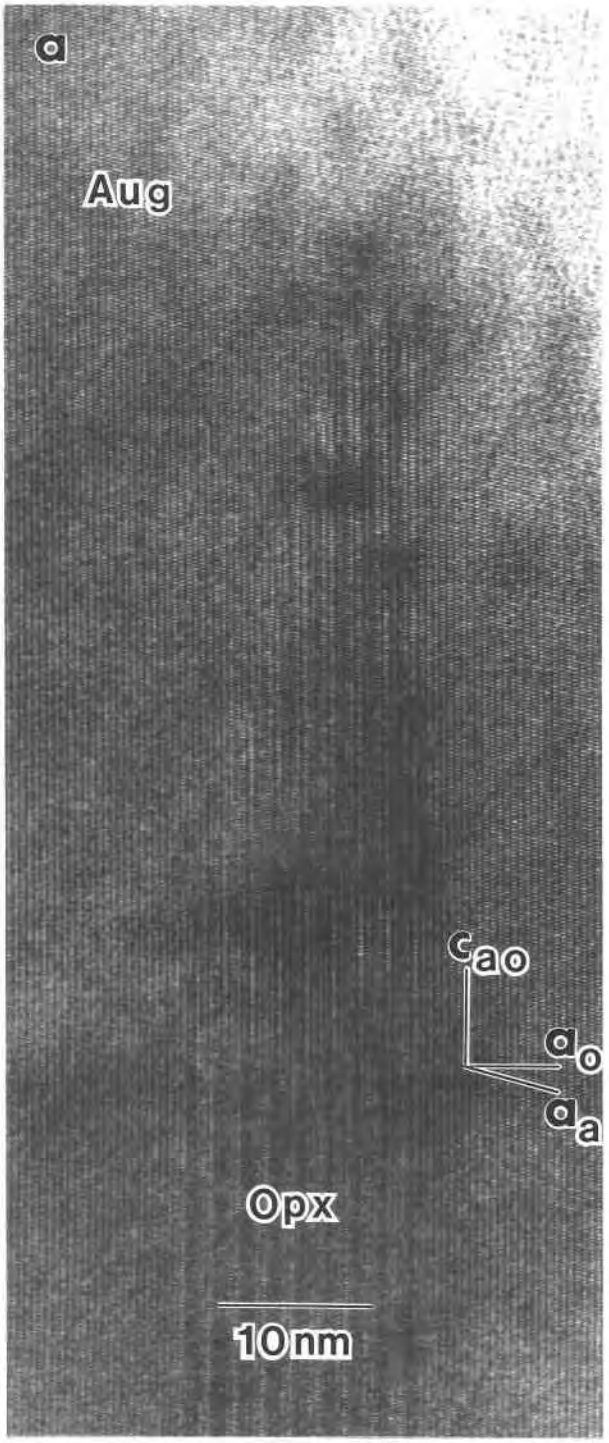

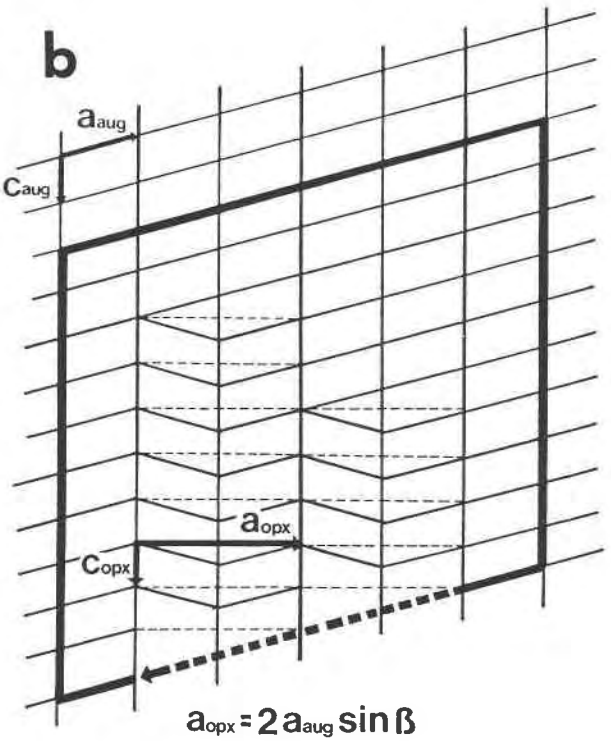

Fig. 9. **(a)** A *b*-axis HRTEM image of the tip of an orthopyroxene lamella in augite. **(b)** Schematic diagram of orthopyroxene growth in augite. The dark line traces a Burgers circuit that shows there is no observable disruption of the augite host.

with highly disordered stacking typically has been based on the assumption that they consist of 0.9-nm slabs.

While most stacking faults and stacking disorder that have been observed in pyroxenes (and other pyriboles) can be described in terms of even-layered fault structures, there is no topological reason why one-layer or other odd-layered faults cannot occur in pyriboles. Odd-layered faults cannot be described in terms of 0.9-nm slabs, but instead require 0.45-nm (100) slabs. Such faults include, for example, (1) faults with $+-+$ structure in clinopyroxenes having the ideal stacking sequence (+) and (2) faults with $+-+$ or $+----+$ structure embedded in otherwise normal orthopyroxene with ideal stacking $(+--+)$.

Although odd-layer faults are structurally permissible (i.e., one can build structure models having such faults with no difficulty), they have not been reported previously. Indeed, in the present study of LAC-6A, the most common stacking faults by far are of the even-layered type, such as the $+--+$ faults in pigeonite shown in Figure 6a. However, as noted above, the short bands of stacking fault between the dissociated partial dislocations in this figure are odd-layered faults having the structure $+-+$. These faults also are peculiar because they are associated with steps in the "001" augite-pigeonite interface and because they separate augite on one side of the fault from pigeonite on the other.

Stacking faults also occur in the orthopyroxene lamellae of LAC-6A. Again, most of these faults are of the even-layered type, but odd-layered faults also occur. The lattice image shown in Figure 10a, obtained under imaging conditions in which dark bands parallel to (100) emphasize the normal 1.8-nm orthopyroxene periodicity, shows both types. The 2.7-nm block of structure (six 0.45-

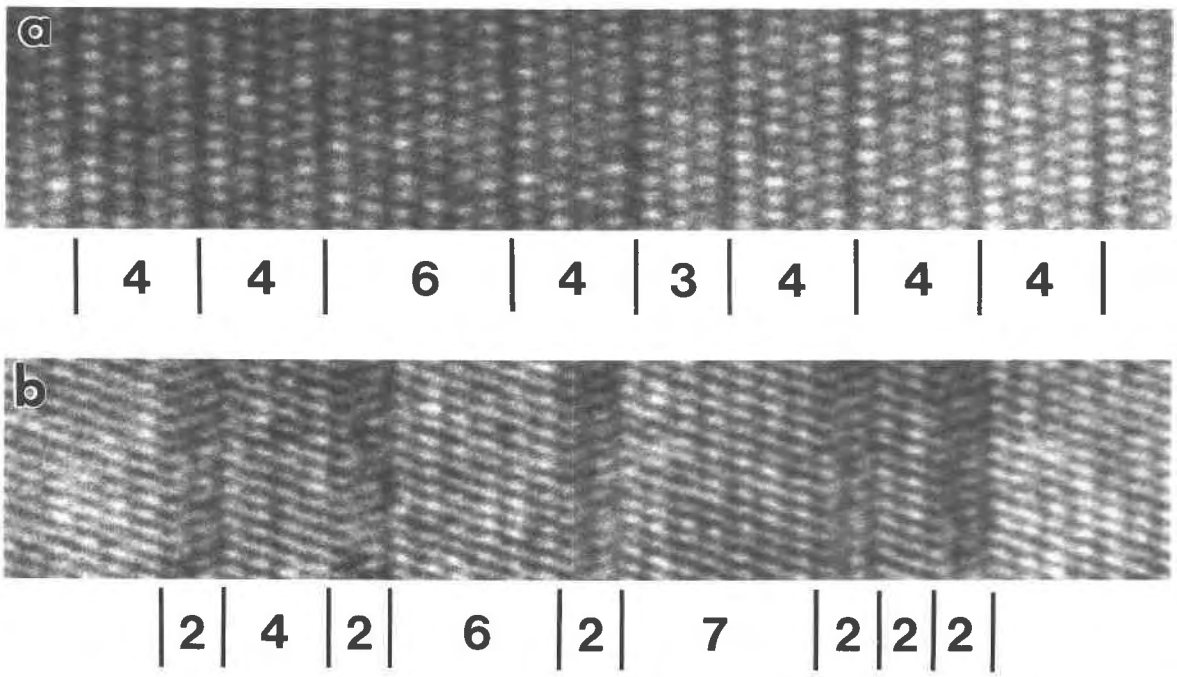

Fig. 10. **(a)** Odd- and even-layered stacking faults in orthopyroxene. Numbers refer to the structural width between dark vertical fringes in units of 0.45-nm (100) layers. All such units in unfaulted orthopyroxene have widths of 4. **(b)** Even-layered faults in pigeonite with odd and even numbers of chains between them.

nm layers) in this figure corresponds to an even-layered fault of the type $+-----+$. (All even-layered faults will produce blocks of structure having widths of $2n \times 0.45$ nm.) Also shown, however, is a 1.35-nm block, which is consistent with an odd-layered fault unit of $+-+$ structure inserted into the orthopyroxene. (All odd-layered faults will produce blocks of structure having widths of $[2n + 1] \times 0.45$ nm.) The low abundance of odd-layered stacking faults, compared to the even-layered types, undoubtedly indicates that they have higher energies under the relatively low temperatures at which most pyroxene microstructures form. At high temperatures in the pure $MgSiO_3$ composition, however, it might be expected that odd-layered faults would occur more commonly, since protoenstatite possesses $+-+$ units as part of its basic $(+-)$ stacking sequence.

It is also observed that the stacking faults in LAC-6A pigeonite lamellae are nearly always separated by regions of pigeonite that are $2n \times 0.45$ nm wide. Out of dozens of observed separations, only two cases were found in which stacking faults were separated by slabs of pigeonite $(2n + 1) \times 0.45$ nm thick; one of these cases is presented in Figure 10b, in which two of the faults are separated by seven 0.45-nm slabs of structure. This observation implies either that (1) the two octahedral sheets of anomalous skew forming the fault always nucleate in the unfaulted pigeonite structure (arrangement a, Table 1), so that they are centered on planes of pigeonite A chains (arrangement b, Table 1), or that (2) they are centered on planes of B chains (arrangement c, Table 1). HRTEM images, such as that in Figure 6a, show that the latter possibility is the one that actually occurs (image interpretation is based on computer-simulated images showing that the more prominent rows of white spots in the image correspond to the layers of A chains, as noted above).

If one considers this type of $+--+$ stacking fault to be a single unit cell of orthopyroxene structure, with the orthopyroxene B chains between the octahedral layers having negative skew, then these observations further imply that the orthopyroxene A chains replace the pigeonite A chains and that the orthopyroxene B chains replace the pigeonite B chains. This structural control on the position of formation of stacking faults in pigeonite may be related to the structural similarities between the pigeonite and orthopyroxene chains: the A chains in both structures are relatively straight, whereas the B chains of both pigeonite and orthopyroxene are more rotated (Cameron and Papike, 1980). These similarities appear to control the stacking-fault positions, in spite of the fact that the pigeonite A chains lie between octahedral layers of like skew, whereas those of orthopyroxene are between layers with opposite skew.

If these $+--+$ stacking faults had formed in a clinopyroxene in which all of the silicate chains were symmetrically identical (e.g., $C2/c$ pigeonite or augite), this structural control would be absent, and the stacking faults (both odd- and even-layered) would be separated by both even and odd numbers of 0.45-nm (100) slabs. This in-

TABLE 1. Consequences of various fault arrangements

a. Unfaulted pigeonite	A + B + A + B + A + B + A + B + A + B
b. Even-layered fault centered on A chains	A + B + A + B − A − B + A + B + A + B | Opx |
c. Even-layered fault centered on B chains	A + B + A + B + A − B − A + B + A + B | Opx |
d. Odd-layered fault without APB	A + B + A + B + A − B + A + B + A + B
e. Odd-layered fault with APB	A + B + A + B + A − A + B + A + B + A ↑ APB

Note: See text for further discussion. A and B indicate the positions of A and B tetrahedral chains, and + and − indicate the skew (stacking vector directions) of the octahedral layers between the silicate chains.

a. Normal pigeonite structure.

b. An even-layered fault consisting of two octahedral layers with anomalous skew, centered on the A chains.

c. An even-layered fault consisting of two octahedral layers with anomalous skew, centered on the B chains. This is the common stacking fault structure in the pigeonite of LAC-6A.

d. An odd-layered fault consisting of a single octahedral layer with anomalous skew.

e. An odd-layered fault consisting of a single octahedral layer with anomalous skew, accompanied by an antiphase boundary with respect to the arrangement of silicate chains. The antiphase boundary is indicated by the juxtaposition of two layers of A chains.

dicates that the stacking faults formed below the pigeonite $C2/c \rightarrow P2_1/c$ phase-transition temperature, which is estimated to be 730 °C for the LAC-6A pigeonite (Livi, 1983). This is consistent with the suggestion of Robinson et al. (1977) that stacking faults in "001" pigeonite lamellae of augites form below the $C \rightarrow P$ transition, as a result of strain induced by changes in unit-cell parameters during cooling.

Odd-layered faults may be less stable than even-layered faults in pigeonite because they place a layer of B chains between octahedral layers of opposite skew (arrangement d, Table 1), although topological constraints force chains in such a position to be relatively straight (Thompson, 1970; Papike et al., 1973; Veblen and Burnham, 1978). It would thus be topologically impossible for this layer of B chains to assume its favored, relatively O-rotated conformation. However, an antiphase boundary (APB) that juxtaposes two A chains might stabilize an odd-layered fault, since it would place the relatively straight chains in both positions where octahedral skew is reversed (arrangement e, Table 1). The rarity of odd-layered faults is consistent with the absence of APBs in the well-annealed LAC-6A pigeonite lamellae. In pigeonites that contain both APBs and (100) stacking faults, we would predict that odd-layered stacking faults would be stabilized by and coincide with APBs parallel to (100).

CONCLUSIONS

We have used conventional TEM observations and HRTEM images interpreted with the aid of computer simulations to elucidate a number of new details about pyroxene interfaces and defect structures. These microstructures formed by exsolution processes during subsolidus equilibration of an augite (LAC-6A) from the Laramie Anorthosite Complex.

The observations confirm that defects such as dislocations and stacking faults can play a critical role in exsolution processes, and they show that there can be great complexity in the ways in which interface morphologies interact with these defects. In addition, interactions between lamellae, probably through their strain fields, can substantially alter the morphology of the lamellae.

HRTEM observations show that stacking faults in pigeonite and orthopyroxene typically involve reversal of the skew of even numbers of octahedral layers. However, odd-layered faults also occur but in lesser numbers, demonstrating that a full description of pyroxene stacking requires the use of (100) slabs that are 0.45-nm thick, as opposed to the 0.9-nm slabs that have been used by some authors. HRTEM images indicating the detailed structures and spacings of stacking faults in the pigeonite lamellae of LAC-6A show that the faults nucleate symmetrically about the B chains of the pigeonite structure. This shows that the detailed conformation of the silicate chains can control the resulting defect structure and that the stacking faults form below the $C2/c \rightarrow P2_1/c$ phase transition as suggested previously.

ACKNOWLEDGMENTS

We thank Gordon Nord and Masao Kitamura for helpful reviews of this paper. We also thank Richard J. Reeder for access to the Stony Brook TEM that was used for the early part of this study, Michael A. O'Keefe for supplying the SHRLI software, Judith Konnert for supplying a modified output routine for these programs, and George Guthrie for his wizardry on the Mac and insightful discussions. This research was supported by NSF grant EAR86-09277. High-resolution microscopy was performed at The Johns Hopkins University using instrumentation obtained with partial support from NSF instrumentation grant EAR83-00365.

REFERENCES CITED

Buseck, P.R., and Iijima, S. (1975) High resolution electron microscopy of enstatite: II. Geological application. American Mineralogist, 60, 771–784.

Buseck, P.R., Nord, G.L., Jr., and Veblen, D.R. (1980) Subsolidus phenomena in pyroxenes. In C.T. Prewitt, Ed., Pyroxenes. Mineralogical Society of America Reviews in Mineralogy, 7, 117–211.

Cameron, M., and Papike, J.J. (1980) Crystal chemistry of silicate pyroxenes. In C.T. Prewitt, Ed., Pyroxenes. Mineralogical Society of America Reviews in Mineralogy, 7, 5–92.

Cameron, M., Sueno, S., Prewitt, C.T., and Papike, J.J. (1973) High tem-

perature crystal chemistry of acmite, diopside, hedenbergite, jadeite, spodumene and ureyite. American Mineralogist, 58, 594–618.

Champness, P.E., and Copley, P.A. (1976) The transformation of pigeonite to orthopyroxene. In H.-R. Wenk et al., Eds., Electron microscopy in mineralogy, p. 228–233. Springer-Verlag, New York.

Champness, P.E., and Lorimer, G.W. (1973) Precipitation (exsolution) in an orthopyroxene. Journal of Materials Science, 8, 467–474.

——— (1976) Exsolution in silicates. In H.-R. Wenk et al., Eds., Electron microscopy in mineralogy, p. 174–204. Springer-Verlag, New York.

Coe, R.S., and Kirby, S.H. (1975) The orthoenstatite to clinoenstatite transformation by shearing and reversion by annealing: Mechanism and potential applications. Contributions to Mineralogy and Petrology, 52, 29–56.

Copley, P.A., Champness, P.E., and Lorimer, G.W. (1974) Electron petrography of exsolution textures in an iron-rich clinopyroxene. Journal of Petrology, 15, 41–57.

Cowley, J.M., and Moodie, A.F. (1957) The scattering of electrons by atoms and crystals: I. A new theoretical approach. Acta Crystallographica, 10, 609–619.

Crawford, S.E., Folks, J.A., Williams, J.A., Barnicoat, A. C., and O'Hara, M.J. (1983) Electron microscope studies of minerals: Phase boundaries in an extremely slowly cooled clinopyroxene (augite). Proceedings of the Royal Society of London, A387, 21–39.

Frost, R., and Lindsley, D.H. (1981) Crystallization conditions of ferrosyenite associated with the Laramie Anorthosite, Wyoming. Geological Society of America Abstracts with Programs, 13, 455.

Fuhrman, M.L., Frost, B.R., and Lindsley, D.H. (1988) Crystallization conditions of the Sybille Monzosyenite, Laramie Anorthosite Complex, Wyoming. Journal of Petrology, 29, 699–729.

Hull, D. (1965) Introduction to dislocations, 259 p. Pergamon, Oxford.

Iijima, S., and Buseck, P.R. (1975) High resolution electron microscopy of enstatite: I. Twinning, polymorphism and polytypism. American Mineralogist, 60, 758–770.

Kitamura, M., Yasuda, M., and Morimoto, N. (1981a) A study of fine textures of Bushveld augite by 200 kV electron microscopy. Bulletin de Minéralogie, 104, 278–284.

——— (1981b) Morphology change of exsolution lamellae of pigeonite in Bushveld augite—An electron microscopic observation. Proceedings of the Japan Academy, Series B, 57, 183–187.

Kohlstedt, D.L., and Vander Sande, J.B. (1976) On the detailed structure of ledges in an augite-enstatite interface. In H.-R. Wenk et al., Eds., Electron microscopy in mineralogy, p. 234–237. Springer-Verlag, New York.

Livi, K.J.T. (1983) Electron microscope investigations of exsolved augites from the ferromonzonite of the Laramie Anorthosite Complex, Wyoming. M.S. thesis, State University of New York at Stony Brook, 172 p.

——— (1987) Geothermometry of exsolved augites from the Laramie Anorthosite Complex, Wyoming. Contributions to Mineralogy and Petrology, 96, 371–380.

Livi, K.J.T., and Veblen, D.R. (1984) Strain-directed growth and coherency in pigeonite exsolution from augite. Geological Society of America Abstracts with Programs, 16, 577.

——— (1987) "Eastonite" from Easton, Pennsylvania: A mixture of phlogopite and a new form of serpentine. American Mineralogist, 72, 113–125.

McLaren, A.C., and Etheridge, M.A. (1976) A transmission electron microscope study of naturally deformed orthopyroxene: I. Slip mechanisms. Contributions to Mineralogy and Petrology, 57, 163–177.

Mori, H., and Takeda, H. (1988) Stress induced transformation of pigeonite from achondritic meteorites. Physics and Chemistry of Minerals, 15, 252–259.

Morimoto, N., and Koto, K. (1969) The crystal structure of orthoenstatite. Zeitschrift für Kristallographie, 129, 65–83.

Müller, W.F. (1974) One dimensional lattice imaging of a deformation induced lamellar intergrowth of orthoenstatite and clinoenstatite [$(Mg,Fe)SiO_3$]. Neues Jahrbuch für Mineralogie Monatshefte, 83–88.

Nobugai, K., and Morimoto, N. (1979) Formation mechanism of pigeonite lamellae in Skaergaard augite. Physics and Chemistry of Minerals, 4, 361–371.

Nord, G.L., Jr. (1980) The composition, structure and stability of Guinier-Preston zones in lunar and terrestrial orthopyroxenes. Physics and Chemistry of Minerals, 6, 109–128.

——— (1982) Analytical electron microscopy in mineralogy: Exsolved phases in pyroxenes. Ultramicroscopy, 8, 109–120.

Nord, G.L., Jr., Heuer, A.H., and Lally, J.S. (1976) Pigeonite exsolution from augite. In H.-R. Wenk et al., Eds., Electron microscopy in mineralogy, p. 220–227. Springer-Verlag, New York.

O'Keefe, M.A., Buseck, P.R., and Iijima, S. (1978) Computed crystal structure images for high resolution electron microscopy. Nature, 274, 322–324.

Papike, J.J., Prewitt, C.T., Sueno, S., and Cameron, M. (1973) Pyroxenes: Comparisons of real and ideal structural topologies. Zeitschrift für Kristallographie, 13, 254–273.

Poldervaart, A., and Hess, H.H. (1951) Pyroxenes in the crystallization of basaltic magma. Journal of Geology, 59, 472–489.

Rietmeijer, F.J.M., and Champness, P.E. (1982) Exsolution structures in calcic pyroxenes from the Bjerkreim-Sokndal lopolith, SW Norway. Mineralogical Magazine, 45, 11–24.

Robinson, Peter. (1980) The composition space of terrestrial pyroxenes—Internal and external limits. In C.T. Prewitt, Ed., Pyroxenes. Mineralogical Society of America Reviews in Mineralogy, 7, 419–494.

Robinson, Peter, Ross, M., Nord, G.L., Smyth, J.R., and Jaffe, H.W. (1977) Exsolution lamellae in augite and pigeonite: Fossil indicators of lattice parameters at high temperature and pressure. American Mineralogist, 62, 857–873.

Salje, E., Kuscholke, B., and Wruck, B. (1985) Domain-wall formation in minerals: 1. Theory of twin boundary shapes in Na-feldspar. Physics and Chemistry of Minerals, 12, 132–140.

Self, P.G., and O'Keefe, M.A. (1988) Calculation of diffraction patterns and images for fast electrons. In P.R. Buseck, J.M. Cowley, and L. Eyring, Eds., High-resolution transmission electron microscopy, p. 244–307. Oxford University Press, Oxford, England.

Smyth, J.R. (1973) An orthopyroxene structure up to 850°C. American Mineralogist, 58, 636–648.

——— (1974) The high temperature crystal structure of clinohypersthene. American Mineralogist, 59, 1069–1082.

Thompson, J.B., Jr. (1970) Geometrical possibilities for amphibole structures: Model biopyriboles. American Mineralogist, 55, 292–293.

——— (1981) An introduction to the mineralogy and petrology of the biopyriboles. In D.R. Veblen, Ed., Amphiboles and other hydrous pyriboles—Mineralogy. Mineralogical Society of America Reviews in Mineralogy, 9A, 141–188.

Vander Sande, J.B., and Kohlstedt, D.L. (1974) A high-resolution electron microscopy study of exsolution in enstatite. Philosophical Magazine, 29, 1041–1049.

Veblen, D.R. (1981) Non-classical pyriboles and polysomatic reactions in biopyriboles. In D.R. Veblen, Ed., Amphiboles and other hydrous pyriboles—Mineralogy. Mineralogical Society of America Reviews in Mineralogy, 9A, 189–236.

Veblen, D.R., and Burnham, C.W. (1978) New biopyriboles from Chester, Vermont: II. The crystal chemistry of jimthompsonite, clinojimthompsonite, and chesterite, and the amphibole-mica reaction. American Mineralogist, 63, 1053–1073.

Manuscript received December 12, 1988
Manuscript accepted June 2, 1989